2017

Tunneling magnetoresistance sensors with different coupled free layers

Yen-Fu Liu

Xiaolu Yin

Yi Yang

Dan Ewing

Paul J. De Rego

See next page for additional authors

Authors

Yen-Fu Liu, Xiaolu Yin, Yi Yang, Dan Ewing, Paul J. De Rego, and Sy-Hwang Liou

Tunneling magnetoresistance sensors with different coupled free layers

Cite as: AIP Advances **7**, 056666 (2017); https://doi.org/10.1063/1.4977774
Submitted: 23 September 2016 . Accepted: 26 November 2016 . Published Online: 01 March 2017

Yen-Fu Liu, Xiaolu Yin, Yi Yang, Dan Ewing, Paul J. De Rego, and Sy-Hwang Liou

Tunneling magnetoresistance sensors with different coupled free layers

Yen-Fu Liu,[1] Xiaolu Yin,[1] Yi Yang,[1] Dan Ewing,[2] Paul J. De Rego,[3] and Sy-Hwang Liou[1,a]
[1]*Department of Physics and Astronomy and Nebraska Center for Materials and Nanoscience, University of Nebraska-Lincoln, Lincoln, Nebraska 68588, USA*
[2]*Department of Energy's National Security Campus, Kansas City, Missouri 64147, USA*
[3]*Department of Energy's National Security Campus, Albuquerque, New Mexico 87106, USA*

(Presented 1 November 2016; received 23 September 2016; accepted 26 November 2016; published online 1 March 2017)

Large differences of magnetic coercivity (H_C), exchange coupling field (H_E), and tunneling magnetoresistance ratio (TMR) in magnetic tunnel junctions with different coupled free layers are discussed. We demonstrate that the magnetization behavior of the free layer is not only dominated by the interfacial barrier layer but also affected largely by the magnetic or non-magnetic coupled free layers. All these parameters are sensitively controlled by the magnetic nanostructure, which can be tuned also by the magnetic annealing process. The optimized sensors exhibit a large field sensitivity of up to 261%/mT in the region of the reversal synthetic ferrimagnet at the pinned layers. [http://dx.doi.org/10.1063/1.4977774]

I. INTRODUCTION

The development of high-sensitivity magnetoresistive sensors involves many practical parameters, such as tunneling magnetoresistance ratio (TMR), coercivity (H_C), exchange-coupling field (H_E), that need to be optimized for the overall performance of the sensors. There are several methods to modify the magnetic properties of the free layer in magnetic tunnel junctions. These methods include using a hard magnet or magnetic field bias, using an orthogonal synthetic-ferrimagnet coupled layer, and using two-step or three-step orthogonal annealing processes.[1–29] The designed shape and geometry of external magnetic concentrators also affect the sensor performance.[30,31]

In this study, we discuss large differences in magnetic coercivity (H_C), exchange coupling field (H_E), and tunneling magnetoresistance ratio (TMR) in magnetic tunnel junctions containing magnetic or non-magnetic coupled free layers. By optimizing the TMR ratio, H_C, H_E, and magnetic flux concentrators, we fabricate an ultra-high-sensitivity magnetic sensor with low dissipative power.

II. EXPERIMENT

The samples are deposited on three-inch thermally oxidized silicon wafers in a magnetron sputtering system with a base pressure of 8 x 10^{-9} Torr and typical deposition pressures in the range of 2-10 mTorr. A MgO tunneling barrier is obtained by rf sputtering of a MgO target at a power of 100 W. The thickness of the MgO barrier is estimated to be about 2 nm based on the resistance-area (RA) product of about 50 kΩ μm^2.[32] The investigated MTJ layer structures (with thicknesses in nanometers) are as follows (see Fig. 1):

[a]sliou@unl.edu; phone 1 402 472-2405; fax 1 402 472-6148

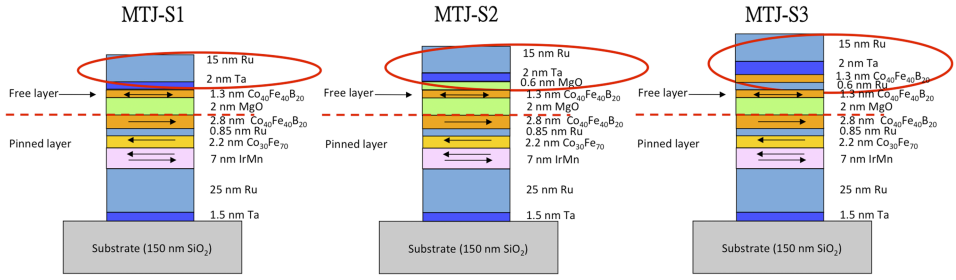

FIG. 1. Schematic MTJ structures with three different designs of free layer: (a) MTJ-S1 1.3 nm $Co_{40}Fe_{40}B_{20}$, (b) MTJ-S2 1.3 nm $Co_{40}Fe_{40}B_{20}$ with additional 0.6 nm MgO layer, and (c) MTJ-S3 1.3 nm $Co_{40}Fe_{40}B_{20}$/0.6 nm Ru/1.3 nm $Co_{40}Fe_{40}B_{20}$.

S1 (1.5 Ta/25 Ru/7 $Ir_{20}Mn_{80}$/2.2 $Co_{30}Fe_{70}$/0.85 Ru/2.8 $Co_{40}Fe_{40}B_{20}$/2 MgO/1.3 $Co_{40}Fe_{40}B_{20}$/2 Ta/15 Ru);

S2 (1.5 Ta/25 Ru/7 $Ir_{20}Mn_{80}$/2.2 $Co_{30}Fe_{70}$/0.85 Ru/2.8 $Co_{40}Fe_{40}B_{20}$/2 MgO/1.3 $Co_{40}Fe_{40}B_{20}$/0.6 MgO/2 Ta/15 Ru);

S3 (1.5 Ta/25 Ru/7 $Ir_{20}Mn_{80}$/2.2 $Co_{30}Fe_{70}$/0.85 Ru/2.8 $Co_{40}Fe_{40}B_{20}$/2 MgO/1.3 $Co_{40}Fe_{40}B_{20}$/0.6 Ru/1.3 $Co_{40}Fe_{40}B_{20}$/2 Ta/15 Ru).

The MTJ junctions were patterned into circles of 30 μm in diameter by photolithography and argon milling. They were then annealed at 350 °C in a magnetic field of 1 T for 1 hour in a vacuum of 2 x 10^{-8} Torr. The annealing magnetic field sets the pinning direction of the pinned layer, along one axis of the circle. The second annealing process was done at 320 °C in 0.1 T for 10 hours. The direction of the 0.1 T magnetic field is perpendicular (90°) to the pinning direction of the pinned layer (in the same plane of pinned layer) to ensure orthogonality between the free layer and the pinned layer. In order to reduce the noise of the sensors, 64 magnetic tunnel junctions were connected into a Wheatstone bridge to form a magnetic field sensor. This magnetic sensor bridge is asymmetric as described in our previous work.[3] As a result of the design, the output signal V_{out} can be amplified by a factor of 2. During the measurement of the sensor performance, the input voltage is 1 V, supplied by batteries to minimize noise. In this study, we used Conetic alloy ($Fe_{16}Ni_{79}Mo_5$) for magnetic flux concentrators (MFC) that were annealed under a pressure of 10^{-7} Torr at 1150 °C for 20 hours with a cooling rate of about 1 °C/min. The saturation induction (B_{sat}) of this annealed conetic alloy is about 0.8 T, maximum permeability (μ_r) reaches about 45,000, and the coercive field (H_c) is about 1.5 μT. The thickness of the external MFC is 1.5 mm, and the gap between two concentrators is about 0.5 mm. All measurements were taken under ambient conditions.

III. RESULT AND DISCUSSION

As shown in Fig. 2, magnetoresistance and applied magnetic field curves were measured along the direction of the easy axis of the pinned layer, which were set after the first annealing

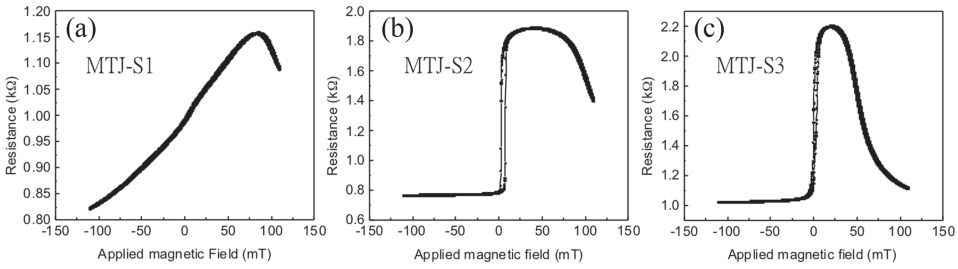

FIG. 2. Magnetoresistance vs. applied magnetic field curves of MTJs with three different designs of free layer: (a) 1.3 nm $Co_{40}Fe_{40}B_{20}$, (b) 1.3 nm $Co_{40}Fe_{40}B_{20}$ with an additional 0.6 nm MgO layer, and (c) 1.3 nm $Co_{40}Fe_{40}B_{20}$/0.6 nm Ru/1.3 nm $Co_{40}Fe_{40}B_{20}$, measured in a magnetic field ranging from -110 mT to +110 mT in the direction of the easy axis of the pinned layer.

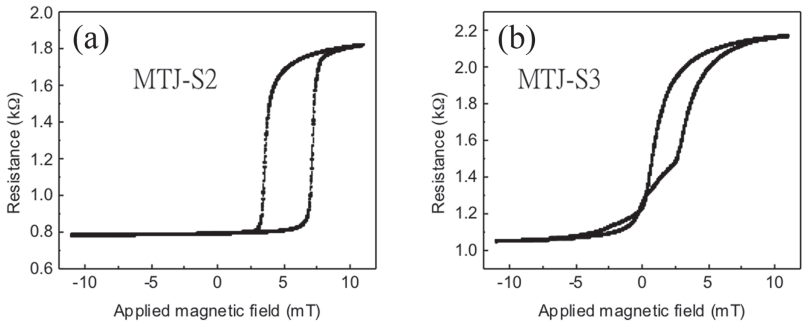

FIG. 3. Magnetoresistance curves of MTJ-S2 and MTJ-S3 measured in a magnetic field varying from -10 mT to +10 mT in the direction of the easy axis of the pinned layer.

process at 350 °C under a 1-Tesla magnetic field for 1 hour. Fig. 2(a) shows the magnetoresistance curve of MTJ-S1 with only a 1.3-nm $Co_{40}Fe_{40}B_{20}$ layer as the free layer. It has no hysteresis in a wide magnetic field range, and the TMR of MTJ-S1 is about 39 %. Fig. 2(b) shows the magnetoresistance curve of MTJ-S2 that has 1.3 nm $Co_{40}Fe_{40}B_{20}$ with additional 0.6 nm MgO added to the free layer. The TMR of MTJ-S2 is about 137% which is much higher than that of MTJ-S1. Fig. 2(c) shows the magnetoresistance curve of MTJ-S3 which has a free layer of 1.3 nm $Co_{40}Fe_{40}B_{20}$/0.6 nm Ru/1.3 nm $Co_{40}Fe_{40}B_{20}$. MTJ-S3 has additional 0.6 nm Ru and 1.3 nm $Co_{40}Fe_{40}B_{20}$ compared with sample MTJ-S1. The TMR of MTJ-S3 is about 120%, slightly less than that of sample MTJ-S2. Both MTJ-S2 and MTJ-S3 have a much smaller saturation field than sample MTJ-S1.

Fig. 3 shows the magnetoresistance curves of MTJ-S2 and MTJ-S3, which were measured in a magnetic field varying from -10 mT to +10 mT in the direction of the easy axis of the pinned layer. The coercivity (H_C) of MTJ-S2 is about 1.7 mT, and the exchange coupling field (H_E) is 5.6 mT. By comparison, MTJ-S3 has a much smaller coercivity H_C (0 -1.0 mT) and a much smaller exchange coupling field (H_E = 1.9 mT) than MTJ-S2. In Table I, parameters related to the overall performance of the sensors are listed, such as tunneling magnetoresistance ratio (TMR), coercivity (H_C), and exchange coupling field (H_E), where TMR is defined as 100% x (R_{max} –R_{min})/R_{min}. In general, the H_C and H_E are evaluated from the middle between R_{max} and R_{min}. For asymmetric resistance as a function of applied magnetic field (such as the MTJ-S3 curve in Fig. 3(b)), we need to evaluate H_C and H_E from several resistance positions (other than the middle between R_{max} and R_{min}). It is clearly shown that the overall magnetic parameters of MTJ-S3 are better than those of all other MTJ samples.

It has been shown previously[30,31] that the magnetic flux concentrators (MFCs) with t-shape, tanga-shape, triangle-shape, and cone-shape are better than concentrators of bar-shape. Our concentrators were designed by combining the t-shape and the triangle-shape. From our previous study,[33] it was also found that the decrease of gap between the two concentrators results in the increase of magnetic flux density. The gap between MFCs in our design, 0.5 mm, could be achieved with a notch added at the tip of each MFC. The magnetic flux density would be amplified about 216 times.

Fig. 4 shows the output voltage as a function of the applied magnetic field for the MTJ-S3 sensor device without MFC (a) and with MFC (b). The input voltage of the sensor is 1 V

TABLE I. Magnetic properties of three magnetic tunnel junctions with different free layers.

	TMR	H_C	H_E
MTJ-S1	39 %	~ 0 mT	–
MTJ-S2	137 %	1.7 mT	5.6 mT
MTJ-S3	120 %	0 ~ 1.0 mT	1.9 mT

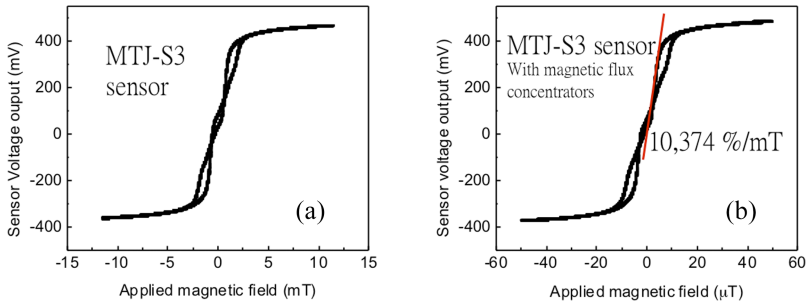

FIG. 4. Output voltage (V_{out}) of the magnetic sensor bridge as a function of the magnetic field in an applied input voltage of 1 V for (a) sensor-S3 (made from MTJ-S3), and (b) sensor-S3 with a pair of MFCs.

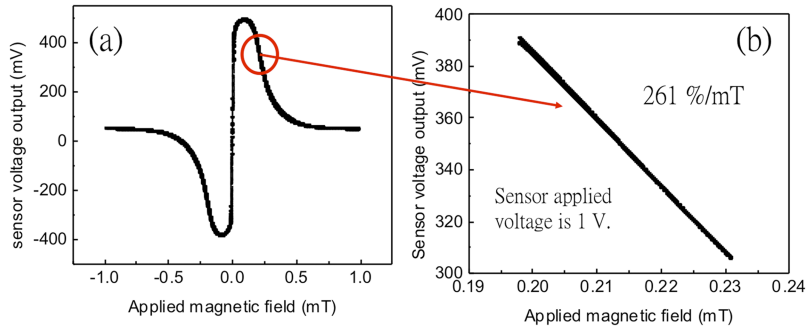

FIG. 5. The output voltage of the sensor as a function of the applied magnetic field in the range of (a) ±1 mT (b) 0.2 mT to 0.23 mT. The magnetic sensor operates under an applied input voltage of 1 V. The sensitivity of this sensor is 261 %/mT at the reversal region of the pinned layer.

supplied by battery. After the integration of MFC, there is no obvious change in the magnetic reversal behavior and the output voltage of the sensor, but the sensitivity of the magnetic sensor is increased by a factor of 216. Fig. 4(b) shows the output voltage of the sensor as a function of the applied magnetic field in the range of ±50 μT. If we use the slope in Fig. 4(b) to calculate the sensitivity, as done by many other groups, the sensitivity of the sensor is about 10,374 %/mT.[6,8,12]

As shown in Fig. 5, this sensor can operate in a very low bias magnetic field (only a few tenths of mT) that corresponds to the reversal region of the pinned layer. In this field region, the magnetization of the free layer is fully saturated (the magnetic noise from the free layer will be reduced). Thus, the sensor is expected to have a smaller magnetic noise. Fig. 5(b) shows a good linear response of the sensor's output voltage as a function of the applied magnetic field in the range of 0.2 mT to 0.23 mT.

IV. CONCLUSIONS

In summary, we have investigated three designs of magnetic tunnel junctions with different magnetic free layer structures. The added layer of 0.6 nm MgO in MTJ-S2 above the 1.3 nm $Co_{40}Fe_{40}B_{20}$ free layer improves the crystalline quality, so that the MR loop exhibits a high TMR. The addition of 0.6 nm Ru and 1.3 nm $Co_{40}Fe_{40}B_{20}$ above the 1.3 nm $Co_{40}Fe_{40}B_{20}$ free layer in MTJ-S3 introduces a ferromagnetic-ferromagnetic exchange coupling with the free layer that improves the overall qualities of MTJ. It has small values of H_C and H_E with a TMR greater than 100%. We also show a new possibility of applying the magnetic sensor in the magnetic field range in which the pinned layer is reversed. The reversal behavior of the $Co_{40}Fe_{40}B_{20}$ in the pinned layer could be a new sensing mechanism for high sensitivity and low noise sensors.

ACKNOWLEDGMENTS

This work was supported by the Department of Defense (Army Research Office) under Awards W911NF-10-2-0099, Honeywell Federal Manufacturing & Technologies. The research was performed in part in the Nebraska Nanoscale Facility: National Nanotechnology Coordinated Infrastructure and the Nebraska Center for Materials and Nanoscience, which are supported by the National Science Foundation under Award ECCS: 1542182, and the Nebraska Research Initiative.

The authors thank Stephen E. Russek and John Moreland at NIST and L. Yuan, M. L. Yan and J. Shen at Western Digital Corporation for their help and useful discussions.

[1] P. P. Freitas, R. Ferreira, S. Cardoso, and F. Cardoso, "Magnetoresistive sensors," J. Phys. Condens. Matter **19**, 165221–165242 (2007).
[2] A. S. Edelstein, G. A. Fischer, M. Pedersen, E. R. Nowak, S. F. Cheng, and C. A. Nordman, "Progress toward a thousandfold reduction in 1 f noise in magnetic sensors using an ac microelectromechanical system flux concentrator (invited)," J. Appl. Phys. **99**, 08B317 (2006).
[3] S. H. Liou, D. Sellmyer, S. E. Russek, R. Heindl, F. C. S. Da Silva, J. Moreland, D. P. Pappas, L. Yuan, and J. Shen, "Magnetic noise in a low-power picotesla magnetoresistive sensor," IEEE Sensors 2009 Conference, 1848–1851 (2009).
[4] R. C. Chaves, S. Cardoso, R. Ferreira, and P. P. Freitas, "Low aspect ratio micron size tunnel magnetoresistance sensors with permanent magnet biasing integrated in the top lead," J. Appl. Phys. **109**, 07E506 (2011).
[5] K. Fujiwara, M. Oogane, S. Yokota, T. Nishikawa, H. Naganuma, and Y. Ando, "Fabrication of magnetic tunnel junctions with a bottom synthetic antiferro-coupled free layers for high sensitive magnetic field sensor devices," J. Appl. Phys. **111**, 07C710 (2012).
[6] J. Y. Chen, N. Carroll, J. F. Feng, and J. M. D. Coey, "Yoke-shaped MgO-barrier magnetic tunnel junction sensors," Appl. Phys. Lett. **101**, 262402 (2012).
[7] S. H. Liou, X. Yin, S. E. Russek, R. Heindl, F. C. S. Da Silva, J. Moreland, D. P. Pappas, L. Yuan, and J. Shen, "Picotesla magnetic sensors for low-frequency applications," IEEE Trans. on Magnetics **47**, 3740–3743 (2011).
[8] M. Pannetier, C. Fermon, G. Le Goff, J. Simola, and E. Kerr, "Femtotesla magnetic field measurement with magnetoresistive sensors," Sci. **304**, 1648–1650 (2004).
[9] D. Wang, J. Daughton, C. Nordman, P. Eames, and J. Fink, "Exchange coupling between ferromagnetic and antiferromagnetic layers via Ru and application for a linear magnetic field sensor," J. Appl. Phys. **99**, 08H703 (2006).
[10] S. Ikeda, J. Hayakawa, Y. Ashizawa, Y. M. Lee, K. Miura, H. Hasegawa, M. Tsunoda, F. Matsukura, and H. Ohno, "Tunnel magnetoresistance of 604% at 300 K by suppression of Ta diffusion in CoFeB/MgO/CoFeB pseudo-spin-valves annealed at high temperature," Appl. Phys. Lett. **93**, 082508 (2008).
[11] F. G. Aliev, R. Guerrero, D. Herranz, R. Villar, F. Greullet, C. Tiusan, and M. Hehn, "Very low 1/f noise at room temperature in fully epitaxial Fe/MgO/Fe magnetic tunnel junctions," Appl. Phys. Lett. **91**, 232504 (2007).
[12] R. C. Chaves, P. P. Freitas, B. Ocker, and W. Maass, "Low frequency picotesla field detection using hybrid MgO based tunnel sensors," Appl. Phys. Lett. **91**, 102504 (2007).
[13] P. W. T. Pong, B. Schrag, A. J. Shapiro, R. D. McMichael, and W. F. Egelhoff, Jr., "Hysteresis loop collapse for linear response in magnetic-tunnel-junction sensors," J. Appl. Phys. **105**, 07E723 (2009).
[14] J. Deak, A. Jander, E. Lange, S. Mundon, D. Brownell, and L. Tran, "Delta-sigma digital magnetometer utilizing bistable spin-dependent-tunneling magnetic sensors," J. Appl. Phys. **99**, 08B320 (2006).
[15] S. H. Liou, R. Zhang, S. E. Russek, L. Yuan, S. T. Halloran, and D. P. Pappas, "Dependence of noise in magnetic tunnel junction sensors on annealing field and temperature," J. Appl. Phys. **103**, 07E920 (2008).
[16] W. Zhang, G. Xiao, and M. J. Carter, "Two-dimensional field-sensing map and magnetic anisotropy dispersion in magnetic tunnel junction arrays," Phys. Rev. B. **83**, 144416 (2011).
[17] B. Negulescu, D. Lacour, F. Montaigne, A. Gerken, J. Paul, V. Marien, J. Marien, C. Duret, and M. Hehn, "Wide range and tunable linear magnetic tunnel junction sensor using two exchange pinned electrodes," Appl. Phys. Lett. **95**, 112502 (2009).
[18] X. Yin and S. H. Liou, "Novel magnetic nanostructured multilayer for high sensitive magnetoresistive sensor," IEEE Sensors 2012 Conference, 2090 (2012).
[19] X. Yin, R. Skomski, D. Sellmyer, S. H. Liou, S. E. Russek, E. R. Evarts, J. Moreland, A. S. Edelstein, L. Yuan, M. L. Yan, and J. Shen, "Adjusting free layer structures of magnetic tunnel junctions for high sensitive magnetoresistive sensors," J. Appl. Phys. **115**, 17E528 (2014).
[20] H. D. Gan, S. Ikeda, W. Shiga, J. Hayakawa, K. Miura, H. Yamamoto, H. Hasegawa, F. Matsukara, T. Ohkubo, K. Hono, and H. Ohno, "Tunnel magnetoresistance properties and film structures of double MgO barrier magnetic tunnel junctions," Appl. Phys. Lett. **96**, 192507 (2010).
[21] Q. L. Ma, S. Lihama, T. Kubota, X. M. Zhang, S. Mizukami, Y. Ando, and T. Miyazaki, "Effect of Mg interlayer on perpendicular magnetic anisotropy of CoFeB films in MgO/Mg/CoFeB/Ta structure," Appl. Phys. Lett. **101**, 122414 (2012).
[22] D. K. Kim, J. U. Cho, B. S. Chun, K. H. Shin, K. J. Lee, M. Tsunoda, M. Takahashi, and Y. K. Kim, "Magnetotransport properties of dual MgO barrier magnetic tunnel junctions consisting of CoFeB/FeNiSiB/CoFeB free layers," Appl. Phys. Lett. **101**, 232401 (2012).
[23] T. Devolder, P. H. Ducrot, J. P. Adam, I. Barisic, N. Vernier, J. V. Kim, B. Ockert, and D. Ravelosona, "Damping of CoxFe80−xB20 ultrathin films with perpendicular magnetic anisotropy," Appl. Phys. Lett. **102**, 022407 (2013).
[24] Y. T. Chen, S. H. Lin, and W. H. Hsieh, "Differential scanning calorimetric determination of the thermal properties of amorphous Co60Fe20B20 and Co40Fe40B20 thin films," Appl. Phys. Lett. **102**, 051905 (2013).
[25] G. Yu, Z. Wang, M. Abolfath-Beygi, C. He, X. Li, K. L. Wang, P. Nordeen, H. Wu, G. P. Carman, X. Han, I. A. Alhomoudi, P. K. Amiri, and K. L. Wang, "Strain-induced modulation of perpendicular magnetic anisotropy in Ta/CoFeB/MgO structures investigated by ferromagnetic resonance," Appl. Phys. Lett. **106**, 072402 (2015).

[26] G. Q. Yu, L. F. Feng, H. Kurt, H. F. Liu, X. F. Han, and J. M. D. Coey, "Field sensing in MgO double barrier magnetic tunnel junctions with a superparamagnetic Co50Fe50 free layer," J. Appl. Phys. **111**, 113906 (2012).
[27] G. V. Swamy, R. K. Rakshit, R. P. Pant, and G. A. Basheed, "Origin of 'in-plane' and 'out-of-plane' magnetic anisotropies in as-deposited and annealed CoFeB ferromagnetic thin films," J Appl. Phys. **117**, 17A312 (2015).
[28] J. Shiha, M. Gruber, M. Kodzuka, T. Ohkubo, S. Mitani, K. Hono, and M. Hayashi, "Influence of boron diffusion on the perpendicular magnetic anisotropy in Ta|CoFeB|MgO ultrathin films," J. Appl. Phys. **117**, 043913 (2015).
[29] L. Gao, X. Jiang, S. H. Yang, P. M. Rice, T. Toruria, and S. S. P. Parkin, "Increased tunneling magnetoresistance using normally bcc CoFe alloy electrodes made amorphous without glass forming additives," Phys. Rev. Lett. **102**, 247205 (2009).
[30] P. M. Drljaca, F. Vincent, P. A. Besse, and R. S. Popovic, "Design of planar magnetic concentrators for high sensitivity Hall devices," Sensors and Actuators A **97-98**, 10–14 (2002).
[31] H. Blanchard, *Hall Sensors with Integrated Magnetic Flux Concentrators, Series in Microsystems* (Hartung-Gorre Verlag, Konstanz, Germany, 1999), Vol. 5.
[32] S. Yuasa, T. Nagahama, A. Fukushima, Y. Suzuki, and K. Ando, "Giant room-temperature magnetoresistance in single-crystal Fe/MgO/Fe magnetic tunnel junctions," Nature Materials **3**, 868–871 (2004).
[33] X. Yin, Y.-F. Liu, D. Ewing, C. K. Ruder, P. J. De Rego, A. S. Edelstein, and S.-Hwang Liou, "Tuning magnetic nanostructures and flux concentrators for magnetoresistive sensors (invited)," Proc. SPIE **9551**, 95512N (2015).